Structure of a Glycerol-Conducting Channel and the Basis for Its Selectivity

Daxiong Fu, Andrew Libson, Larry J. W. Miercke, Cindy Weitzman, Peter Nollert, Jolanta Krucinski, Robert M. Stroud*

Membrane channel proteins of the aquaporin family are highly selective for permeation of specific small molecules, with absolute exclusion of ions and charged solutes and without dissipation of the electrochemical potential across the cell membrane. We report the crystal structure of the *Escherichia coli* glycerol facilitator (GlpF) with its primary permeant substrate glycerol at 2.2 angstrom resolution. Glycerol molecules line up in an amphipathic channel in single file. In the narrow selectivity filter of the channel the glycerol alkyl backbone is wedged against a hydrophobic corner, and successive hydroxyl groups form hydrogen bonds with a pair of acceptor, and donor atoms. Two conserved aspartic acid–proline–alanine motifs form a key interface between two gene-duplicated segments that each encode three-and-one-half membrane-spanning helices around the channel. This structure elucidates the mechanism of selective permeability for linear carbohydrates and suggests how ions and water are excluded.

Members of the aquaporin family (AQPs) are composed of functionally distinct subgroups that include transmembrane water-conducting channels (aquaporins) and glycerol-conducting channels (aquaglyceroporins) that include the *E. coli* glycerol facilitator (GlpF) (*1*–*3*). The electrochemical potential across the cell membrane is preserved by sharp selectivity that excludes all ions including hydroxide, and hydronium ions (*4*). GlpF also conducts linear polyalcohols (called alditols), for which it is stereo- and enantio-selective (*5*).

Found in species from bacteria to yeast, plants, and humans, the sequences of more than 150 AQPs are known. This ancient family arose by tandem intragenic duplication (*6*), resulting in proteins that have an internal repeat where the NH_2-terminal segment displays ~20% conservation with the COOH-terminal segment (*7*). Each segment contains a conserved Asn-Pro-Ala signature sequence (NPA) near its center. Human family members include at least 10 aquaporins (AQP0 to AQP9), all of which are permeable to water. AQP3, AQP7, and AQP9 are also permeable to glycerol. In eukaryotes many of the family members are regulated by phosphorylation, pH, osmolarity, or binding of other proteins or ligands (*8*, *9*).

The first AQP to be characterized was a water-conducting channel, AQP1 (*1*). Monomers of AQP1 assemble in membranes as tetramers of four independent channels (*10*). In reconstituted membranes, the tetramers come together alternately cytoplasmic and extracellular side up. Electron crystallography of AQPs (*11*–*15*) at increasing resolutions down to 4.5 Å in-plane, 4.5 by ~9 Å in three dimensions (*16*) reveals a right-hand twisted arrangement of six transmembrane and two half-membrane–spanning α helices around a central channel (*17*).

The rate of GlpF-mediated glycerol influx is 100- to 1000-fold greater than expected for a transporter and is nonsaturable to a glycerol concentration of >200 mM (*5*). GlpF acts as a highly selective channel, as indicated by lack of counterflow of radioactive substrate against a concentration gradient (*18*).

GlpF structure. The structure of GlpF was determined by isomorphous replacement and anomalous dispersion (Table 1). GlpF crystallizes as a symmetric arrangement of four channels with three glycerol molecules (G1 to G3) in each (Fig. 1, A and B). The plane of the bilayer would be perpendicular to the fourfold axis. Each tetramer is circled by a hydrophobic surface matching the dimensions of the lipid bilayer. The periplasmic leaflet is indicated by the interactions of 12 octylglucoside molecules. Layers that include tryptophan side chains can productively interact with the lipid head-group regions and are capped by charged residues that result in net positive charge on the cytoplasmic side consistent with the trend in other membrane proteins.

Six transmembrane and two half-membrane–spanning α helices (M1 to M8) form a right-handed helical bundle around each channel. The helices M1 to M8 diverge outward from the central plane to generate a vestibule on each surface. The interhelix angles of ~+35° to +40° are not in the categories most favored by "knobs into holes" packing (*19*). However, helices pack with near optimal packing angles of ~−20°, both between M1 and M2 of one monomer and M5 and M6 of its neighbor, and between (four copies of) M2 and M6 of all monomers around the fourfold axis.

The NH_2-terminus of GlpF was found to be cytoplasmic by thrombin accessibility, as in AQP1 (*20*). The two genetic repeats form segments related by a quasi twofold axis that would pass through the center of the bilayer and intersect the fourfold axis. The NH_2-terminal segment begins with two membrane-spanning helical segments, M1 and M2, followed by residues 61 to 67 that project into the center of the channel as an extended polypeptide chain and provide three successive carbonyls to the cytoplasmic vestibule. The half-spanning helix M3 begins with the first NPA motif and returns to the cytoplasmic side. M4 is packed between M3 and M1 (Fig. 1, B and D).

The COOH-terminal segment reiterates a similar transmembrane topology beginning from the periplasmic side that likewise provides three carbonyls to the periplasmic vestibule from the extended chain 195–202. Thus, the quasi twofold relation applies to elements of the amphipathic walls of the channel. The acceptor carbonyls in the vestibules, and the hydrogen bond donors of Arg^{206}, Asn^{68}, and Asn^{203} at the interface of the two half-helices M3 and M7 form a left-handed helical polar stripe that connects the periplasmic and cytoplasmic vestibules. The region that links the two segments forms two short α helices (109–120 and 126–134) that are protrusions on the periplasmic side at the COOH-terminal end of M4. An extended chain (137–143) returns to the walls of the channel and contributes three more carbonyls to the periplasmic vestibule.

A unique feature of this membrane protein structure is that two helices meet at their NH_2-terminal ends in the center of the membrane. Their conserved NPA motifs create an intimate interface across the quasi twofold axis in which the proline rings are in Van der Waals contact cupped between the proline and alanine side chains of the opposite helix (Fig. 1C). Each asparagine side chain is constrained by two hydrogen bonds that precisely orient side-chain NHs toward acceptors on the permeant substrate. One side of each half-spanning helix M3, M7 contacts the lipid-accessible exterior perimeter of the tetramer. The helical axes of M3, M7 intersect at an angle of ~146°, thereby narrowing the cross section of the channel in the center of the bilayer region.

Two transmembrane helices, M2 and M6,

Department of Biochemistry and Biophysics, School of Medicine, University of California, San Francisco, CA 94143–0448, USA.

*To whom correspondence should be addressed. E-mail: stroud@msg.ucsf.edu

positioned nearest the fourfold axis of the tetramer are not long enough to span the bilayer, consistent with the tetramer being the stable physiological quaternary structure. The interfaces between subunits are almost as hydrophobic as the exterior, suggesting that a monomer could be transiently stable in the membrane upon synthesis, before forming tetramers.

The high conservation throughout the aquaporin family indicates functional and structural roles in the context of a common fold (Table 2). Of eight residues that are conserved in the two repeats (group III), six lie close to the central plane of the bilayer related by the quasi twofold axis of symmetry to corresponding residues in the second repeat. They contact each other in pairs and maintain packing around the narrow region of the channel and around the quasi twofold axis in GlpF. Four of these are glycines within helices that allow the closest approaches of helices in the center of the bundle (*21*).

The channel. The channel has a ~15 Å wide vestibule on the periplasmic surface and

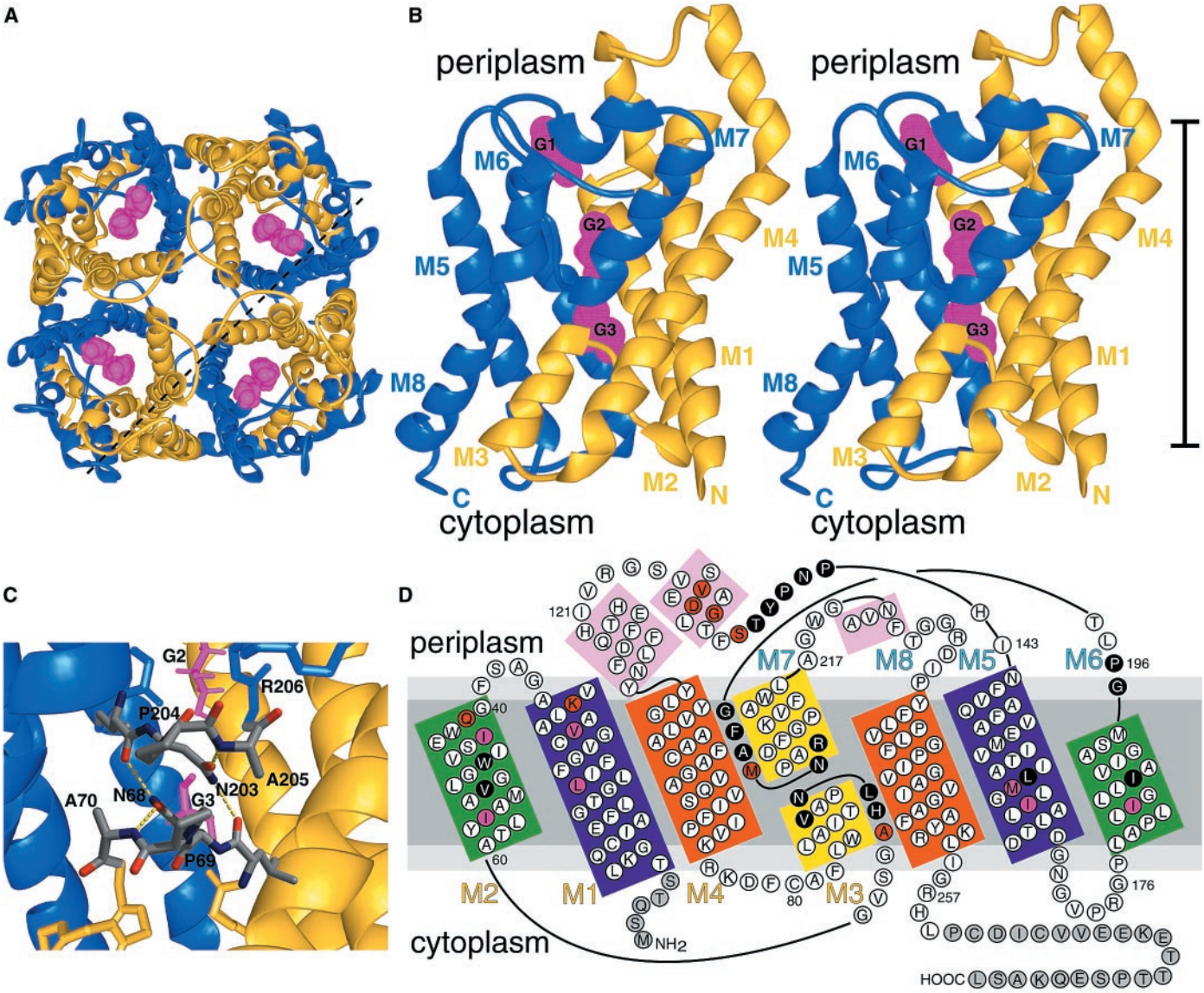

Fig. 1. Three-dimensional fold of GlpF with the quasi twofold related segments colored in yellow (residues 6 to 108) and blue (residues 144 to 254). Glycerols G1, G2, and G3 lined up within the channel pathway are colored magenta. (**A**) Ribbon representation of the GlpF tetramer viewed from the periplasmic side. The dotted line represents the clipping plane used in Fig. 2B. (**B**) A stereo view (crossed eyed) of the monomeric glycerol channel viewed down the quasi twofold axis. The vertical bar (35 Å) represents the position of the membrane. Helices are labeled M1 to M8. (**C**) The two NPA motifs at the segment interface where the two half-helices M3 (yellow) and M7 (blue) meet form a clasplike junction. Each proline ring lies in-between the proline and alanine side chains of the opposite helix. The asparagine amide groups of one helix form two symmetry-related hydrogen bonds—one with the alanine nitrogen of that same half-helix and one with a carbonyl oxygen of the opposite half-helix. This structure presents a highly constrained pair of donor hydrogen bonds to successive OHs at G3. In this and succeeding figures, atoms are colored according to atom type (oxygen, red; carbon, gray; nitrogen, blue; and sulfur, yellow). (**D**) The amino acid sequence of GlpF is arranged topologically as in the structure, with helices viewed as if from inside the channel, viewed looking away from the fourfold axis. The NPA motifs are in the center of the figure. Three-and-one-half helices compose each segment, labeled M1 to M4 and M5 to M8. Related helices M1 and M5, M2 and M6, and so forth are boxed in similar colors to represent their homologous roles in the structure. Residues in black circles interact with glycerol. Residues in red circles contribute carbonyl oxygen or amide NHs to the channel. Residues in purple circles contribute hydrocarbon to the channel. Gray circles represent residues that are not seen in the structure. The deduced location of the cell membrane is illustrated in gray. Abbreviations for the amino acid residues are as follows: A, Ala; C, Cys; D, Asp; E, Glu; F, Phe; G, Gly; H, His; I, Ile; K, Lys; L, Leu; M, Met; N, Asn; P, Pro; Q, Gln; R, Arg; S, Ser; T, Thr; V, Val; W, Trp; and Y, Tyr.

reaches its constriction of ~3.8 Å by 3.4 Å, 8 Å above the quasi twofold axis. This constriction lies at the start of a ~28 Å long selective channel (radius <3.5 Å) that extends to the cytoplasmic surface (Fig. 2). G1 is hydrogen bonded to the O of Tyr^{138} in the entry vestibule. G2 and G3 are both tightly organized in a site we term the "selectivity filter," a region only large enough in cross section to accommodate a single CH-OH group (Fig. 3). Therefore, CH-OH groups of alditol molecules can only pass through the region of G2 and G3 in single file. The water molecule between G2 and G3 suggests that, at least at high concentrations of glycerol, glycerol and water may be stoichiometrically cotransported.

The selectivity filter is strongly amphipathic, with the planes of two perpendicular aromatic rings (Trp^{48} and Phe^{200}) forming a hydrophobic corner (Fig. 3A). The alkyl backbone of G2 is tightly packed against this corner, leaving no space for any substitution at the C-H hydrogen positions. The O1 and O2 (Fig. 3B) of G2 are each both hydrogen bond acceptors from successive NHs of the guanidinium group of Arg^{206} and hydrogen bond donors to the carbonyl oxygens of Gly^{199} and Phe^{200}, respectively (Fig. 3C). These carbonyls, and that of Ala^{201}, are oriented on the periplasmic side of the selectivity filter by hydrogen bonding from main-chain amide NHs of Phe^{200}, Ala^{201} to the buried COOH of invariant Glu^{152}. The negative charge of Glu^{152} mediated by the amides of Phe^{200} and Ala^{201}, and the positive charge on Arg^{206} form an "electrostatic triangle" that polarizes each of two successive OH groups on a permeant alditol. This implies that any permeant molecule should also be polarizable in section parallel to the plane of the membrane.

G3 straddles the constrained hydrogen bond donor NH group of Asn^{203}, and Asn^{68} between M3 and M7. The NH_2 of Asn^{203} forms a hydrogen bond with O1 of G3 with ideal geometry. The NH_2 of Asn^{68} hydrogen bonds with O2 of G3 also with ideal geometry, whereas the carbonyl of highly conserved His^{66} is an acceptor for OH3. G2 and G3 have the same handedness, consistent with their lying on a pathway that conducts glycerol without rotation about the horizontal axis as it is transported.

The carbonyls of His^{66}, Ala^{65}, and Gly^{64} on the cytoplasmic side are quasi twofold related to the carbonyls of Ala^{201}, Phe^{200}, and Gly^{199} on the periplasmic side. They are oriented on the cytoplasmic side by hydrogen bonding of backbone NHs to a second highly conserved buried carboxyl, Glu^{14}. This creates a helical line of six hydrogen bond acceptors that define the polar side of the amphipathic channel (Fig. 2B).

Glycerol becomes progressively dehydrated in the periplasmic vestibule to move through the selectivity filter by exchanging

Table 1. Crystallographic statistics to 2.2 Å resolution. GlpF, which includes an NH_2-terminal six-histidine tag followed by a thrombin cleavage site, was cloned from *E. coli* strain K12 and purified by nickel affinity and size-exclusion chromatography. GlpF (15 to 20 mg/ml) was crystallized from a solution that contained 28% (w/v) polyethylene glycol 2000, 100 mM Bicine, 15% (v/v) glycerol, 35 mM *n*-octyl-β-D-glucoside, 300 mM $MgCl_2$, and 5 mM dithiothreitol (DTT) (pH 8.9). Crystals were in space group *I*422 (a = 96.4 Å, c = 184.5 Å). Data were collected at ALS beamline 5.0.2 with a charge-coupled device detector (Quantum) and integrated and scaled with MOSFLM and SCALA (*37*). Phases were calculated by multiple isomorphous replacement (MIR) and anomalous scattering with SHARP (*38*). After solvent flattening and phase extension to 3.0 Å, the initial map showed a single, continuous, main-chain density with strong side-chain features that allowed unambiguous sequence assignment for 80% of the residues in GlpF. The model was completed and refined with CNS (*39*). PCMBS, P-chloromercuribenzene sulfonate.

Data collection				
Data set	Native	PCMBS	Tl-K-Cl	F-HgAc
Wavelength (Å)	1.1	1.0	1.0	1.0
Resolution (Å)	2.2	3.2	3.0	3.0
Observations	139,069	16,758	35,297	58,110
Unique	19,141	4,620	7,540	7,527
Completeness (%)	90.9 (57.7)	65.5 (22.7)	90.9 (41.6)	92.0 (47.5)
R_{sym} (%)	7.4 (39.3)	8.2 (15.3)	4.4 (11.3)	8.5 (19.1)
$I/\sigma I$	15.8 (1.7)	10.0 (1.6)	21.2 (5.3)	17.2 (3.5)
MIR analysis				
Resolution cutoff (Å)		4.0	4.0	5.0
Number of sites		2	2	2
Phasing power (iso/ano)		2.6/1.5	2.3/0.8	2.9/2.0
R_{Cullis}		0.74	0.74	0.67
Overall figure of merit to 4 Å = 0.62				

Refinement statistics	
No. of reflections (working/test)	16750/1966
No. of nonhydrogen atoms	2085
Unobserved residues	1 to 5, 260 to 281
Resolution (Å)	20 to 2.2
R_{cryst}/R_{free} (%)	19.7/22.3
Average B factor (Å^2)	28
Model geometry	
Bond length deviation (Å)	0.006
Bond angle deviation (°)	1.2

Table 2. Sequence-structure relationship in GlpF. The roles of the most conserved residues, based on sequence alignment of 52 representative aquaporin family members (*3*). Group I includes residues found only in the first genetic repeat; group II, residues in the second repeat only; and group III, residues conserved in both repeats I and II. Group I and II therefore may be related to structure and function specific to each respective repeat, whereas group III reflects the symmetric relation between the two genetic repeats.

Residues	Conservation (%)	Role in the structure
	Group I	
S63	92	Packing core near N68
H66	96	Packing core near N68
V71	87	Packing core near N68
T72	88	Packing core near N68
Y89	92	Packing core near N68
Q93	100	Packing core near N68
	Group II	
L159	85	Channel wall near G3
R206	92	Selectivity filter G2
P240	90	Packing core near N203
	Group III	
E14/E152	90/85	Buried, binds, and orients the vestibule
T18/T156	83/87	Mid-membrane plane
G49/G184	82/94	Mid-membrane plane
G96/G243	98/44	Mid-membrane plane
G64/G199	94/6	Buried, binds, and orients the vestibule
NPA (68-70)/ NPA (203-205)	100	Mid-membrane plane, and G3

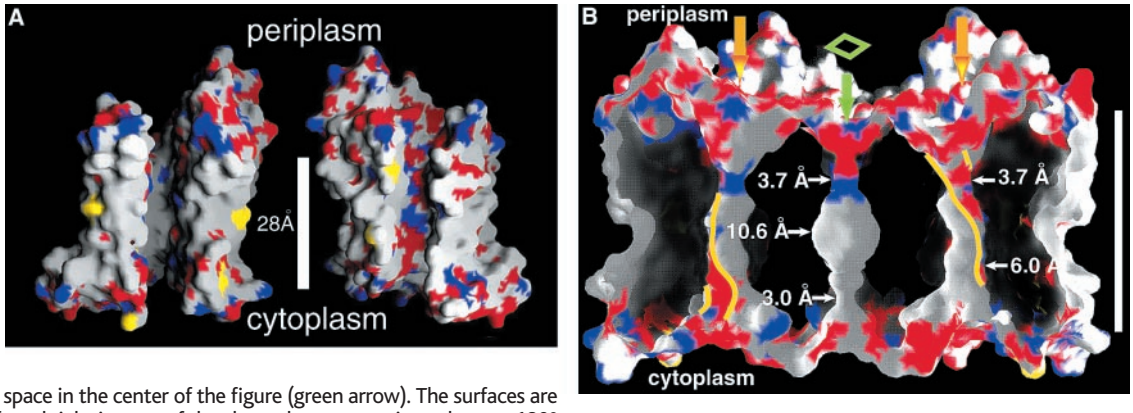

Fig. 2. The glycerol-conducting channel in GlpF. (**A**) The surface of the glycerol channel is colored according to atom type, showing the hydrophobic surface (left) and the polar surface (right). The length of the narrow region through the channel is indicated by the bar. (**B**) The GlpF tetramer sectioned diagonally as indicated by the dotted line in Fig. 1A in front of the plane containing the two glycerol channels indicated by orange arrows, and the fourfold axial space in the center of the figure (green arrow). The surfaces are colored by atom type. The left and right images of the channel represent views that are 180° apart. The left-handed helical stripe corresponding to the amphipathic pathway through the channel is indicated by orange lines. A 35 Å vertical bar indicates the deduced position of the bilayer. Cross-section widths of the glycerol channel and space around the fourfold axis are indicated.

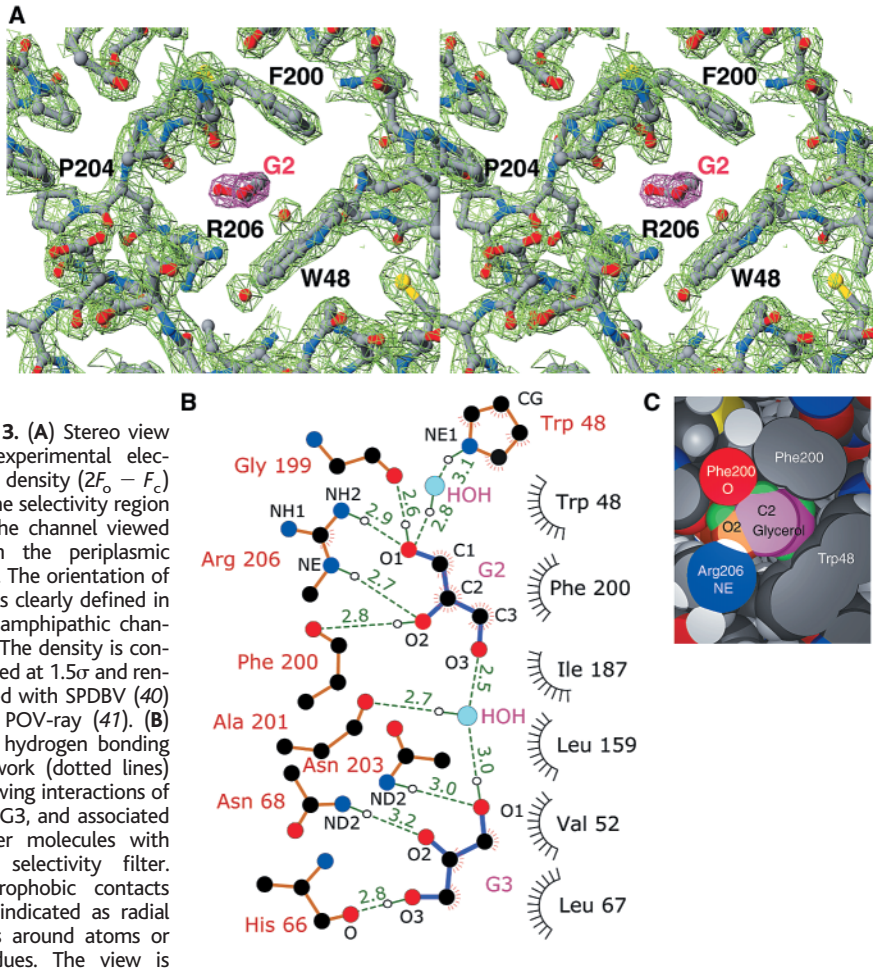

Fig. 3. (**A**) Stereo view of experimental electron density ($2F_o - F_c$) in the selectivity region of the channel viewed from the periplasmic side. The orientation of G2 is clearly defined in the amphipathic channel. The density is contoured at 1.5σ and rendered with SPDBV (*40*) and POV-ray (*41*). (**B**) The hydrogen bonding network (dotted lines) showing interactions of G2, G3, and associated water molecules with the selectivity filter. Hydrophobic contacts are indicated as radial lines around atoms or residues. The view is rotated 90° about a vertical axis from the view in Fig. 1B. Distances (in angstroms) between heavy atoms are indicated. (**C**) Cross section through the channel (space-filling rendering) showing the interactions with G2OH2, O2 (orange) and its associated CH group (C2; purple), and hydrogen (green). The cross section shows the donor NEH of Arg^{206}, acceptor carbonyl oxygen of Phe^{200}, and hydrophobic corner formed by Trp^{48} and Phe^{200} viewed edge-on to the aromatic rings.

one set of stringent hydrogen bonds for another. The pathway can be visualized as a series of activation barriers that separate intermediate binding sites through the channel, including the ones we observe at G2 and G3 (*22*). The narrowest constriction in the channel lies in between G1 and G2. Thus, it constitutes a putative "transition state" in the pathway. At this narrowest position the hydrogen bond geometry from the donor NHη of Arg^{206} to an OH group would become ideal. Thus, it acts as in an enzyme to lower the activation energy, in this case for transport through the most restricted region.

Stereoselective preference for glycerol and linear carbohydrates. To assess the selectivity of GlpF we adapted an osmotic method (*23*) to measure influx of carbohydrates into reconstituted proteoliposomes (Fig. 4). Upon addition of carbohydrates, proteoliposomes shrink owing to osmosis. The rate of carbohydrate influx is indicated by the rate of recovery of the initial volume of proteoliposomes. Ribitol, with all OH groups having the same stereospecific relation to the carbon backbone, generated an exponential reswelling with a time constant of ~2.9 s (Fig. 4, inset). In contrast D-arabitol, a chiral stereoisomer of ribitol with a mixed arrangement of hydroxyls, shows a ~10-fold reduction in transport relative to ribitol, demonstrating stereoselectivity of the channel. The structure shows how this can be visualized because two successive –CHOH groups are oriented at the G2 site. The carbon backbone must be lined up along the channel axis. Depending on the enantiomer, the C-H hydrogen(s) is in contact with the aromatic ring of either Phe^{200} or Trp^{48} in similar environments. However, any CHOH groups adjacent to these two will place the carbon in one of two tetrahedrally disposed sites that have quite different environments. The permeation of D-arabitol is slowed considerably, most likely owing to the difference in accommodation at these adjacent positions. There must therefore be some selectivity, even between either of the two prochiral (chirality with respect to direction in which the alditol enters the channel) carbon orientations.

Membranes have a high intrinsic permeability for glycerol. When GlpF is present, the reswelling rate increases such that the vesicles recover by a factor similar to that seen with ribitol. Measured as a function of the amount of GlpF used in the reconstitu-

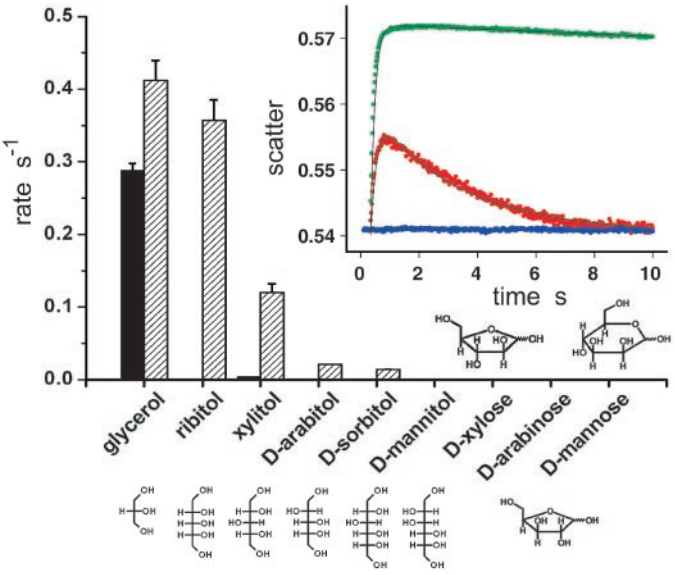

Fig. 4. Relative rates (μ) for conductance of a selection of carbohydrates into protein-free liposomes (black bars) and into GlpF-containing proteoliposomes (hatched bars). Structures are indicated in the Fisher diagrams. Error bars represent the standard deviation from 10 stopped-flow accumulations. (**Inset**) An example of the stopped-flow assay that measures rates of transport of different carbohydrates into reconstituted vesicles, applied in this example to ribitol, a conducted alditol. Vesicles were reconstituted with GlpF (red) or without GlpF (green) and then treated with 100 mM carbohydrate at time $t = 0$, or with buffer at time $t = 0$ (blue), and the change in vesicle size monitored by light scattering at 440 nm. Vesicle size initially decreases rapidly as water diffuses through the lipids in response to the osmotic challenge. The vesicles reswell with a time constant that depends on conductivity. Changes in light scattering Y were therefore fitted by two exponentials. $Y = [A_w(1 - e^{-\lambda t}) - a_0](e^{-\mu t}) + a\infty$. The first time-constant corresponds to the rapid water efflux ($\lambda > 5\ s^{-1}$). The second corresponds to the slower rate of reswelling with time constant μ. The black lines represent the computed fits based on these two exponentials. The time course for a nonconducted alditol, mannitol, into GlpF-containing proteoliposomes lacks any reswelling phase. The reswelling rate due to glycerol influx depends linearly on the amount of GlpF over the entire range of molar ratios of lipid to tetrameric complex tested (950 $-$ ∞). Liposomes with and without GlpF were formed by dilution (*42*, *43*) into reconstitution buffer (20 mM Hepes, pH 7.2) containing 2 mM DTT as described for aquaporins (*27*, *44*). A molar ratio of 14,000 lipids (total acetone/ether-extracted *E. coli* polar lipids; Avanti) to 1 GlpF tetramer (90 mg of lipid/1 mg GlpF) was routinely used unless otherwise specified. After formation and centrifugation, liposomes were extensively dialyzed against reconstitution buffer for the first day with 2 mM DTT and for 3 days without DTT. Light scattering was measured with a Kin Tek stopped-flow model SF-2001 at 25°C. Vesicle diameters were 130 $\pm$ 20 nm as measured by electron microscopy and 138 nm $\pm$ 36 nm as measured by dynamic light scattering with a DynaPro 801 from Protein Solutions.

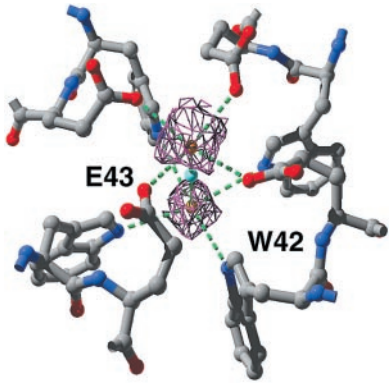

Fig. 5. The center of the tetrameric GlpF complex. At one portion only along the fourfold axis, near the periplasmic surface, there is excess electron density adequately fitted as three oxygens (B = 25, 23, 38 Å^2). This region is more prone to accumulation of higher noise due to symmetry. However, the ($F_o - F_c$) difference map contoured at 1.5σ shows residual positive density at two positions. Therefore, these were treated as two magnesium ions separated by water.

tion, the rate increases proportionately, indicating that transport is a GlpF-dependent process. The rates for a series of alditols demonstrate stereoselectivity of the channel. Of those tested, chiral molecules had lower rates than nonchiral molecules. The rates we observed precisely follow the trend observed for GlpF in whole cells (*5*), showing that in vivo characteristics are represented in reconstituted proteoliposomes.

Selectivity for glycerol versus water. GlpF has a much lower conductivity for water than do water channels (*2*). In GlpF conductivity for water may be impaired by the hydrophobic wall of the channel. The geometric requirements for hydration of water are stringent with typically four or five coordinate waters (*24*, *25*). To pass the filter in single file, waters could not retain more than two water molecules as neighbors, and thus the energetic barrier for such dehydration is high.

Water channels conduct water and not glycerol; however, the side chains that form the hydrophobic corner are smaller and more polar. Trp^{48} is typically replaced by Phe or His; Phe^{200} is typically replaced by Ala, Thr, or Cys. The larger size of the channel should allow a greater degree of water coordination than in GlpF. Replacement of the indole of Trp^{48}, and the phenyl ring of Phe^{200}, also removes the hydrophobic corner so that there is no longer the potential for Van der Waals interaction with the alkyl chain of glycerol, consequently disfavoring alditol transport by water AQPs.

In AQP1, mercury blocks water transport at the thiol of C189 (*26*). The homolog of C189 in GlpF is Phe^{200}, which lies at the narrowest position of the channel. Water transport has also been inactivated by substitution of the counterpart of Arg^{206} in AQPZ (Arg^{189}) by Val or Ser (*27*). A mutation of this residue in human AQP2 causes nephrogenic diabetes insipidus. Although it has been suggested that the disease may be caused by impaired intracellular membrane traffic on the basis of expression in *Xenopus* oocytes (*28*), any mutation here must alter the water transport in the principal cells of the collecting duct in the kidney.

Regulated ion channels formed by AQPs. Certain AQPs act as ion channels under regulated conditions. Cation conductance has been induced in AQP1 by activation of cyclic GMP–dependent pathways (*8*, *29*). In the latter case, cation conductance was blocked by Hg^{2+}, suggesting that a conformational change induced in AQP1 can lead to cation conductance through the normal water channel. AQP6 conducts anions at pH's below 5.5. However, Hg^{2+} leads to an increase in water and anion conductance (*30*), suggesting a different mechanism.

The fourfold symmetry axis: A potential ion channel in AQPs. Electron density on the fourfold axis, near the periplasmic surface, suggests coordination of two cations. The most external is coordinated octahedrally by four glutamates (Glu^{43}, 2.9 Å) and water (2.1 Å) (Fig. 5). The most internal lies in between four indole nitrogens of Trp^{42} (3.6 Å) and 2.3 Å from the water. The electrostatics, bond lengths, and the presence of 300 mM Mg^{2+} suggest that the extra electron densities correspond to Mg^{2+} ions. The remainder of the pathway is surrounded by aliphatic side chains (Fig. 2B). This pathway is notable because many multimeric channels form ion channels on their symmetry axis. The dimensions along the axis are similar to those of the tetrameric, KcsA potassium channel (*31*). Like the KcsA channel, it also has a hydrophobic ~10 Å diameter cavity in the center of the bilayer and, overall, the axial pathway in GlpF is ~10 Å shorter than in the KcsA channel. However, the narrow cytoplasmic vestibule in KcsA is polar, whereas in GlpF it is nonpolar, closing it to all hydrated ions and polar molecules larger than water. Nevertheless, this pathway must be considered as a possible candidate for an ion channel in regulated AQPs.

Maintaining an electrochemical gradient. The channel in GlpF is too narrow to accommodate a hydrated ion, and the energetic cost of removing even a single water of hydration from an ion is prohibitive. Cation channels achieve

selective conductance—for example, in the case of the KcsA or gramicidin channels, by provision of multiple oriented carbonyl groups that each carry a δ^- charge, within narrow selective regions. These can replace or compensate for waters that are displaced from the first hydration shell (*32–36*).

Removal of water from, and fixation of a specific conformation of glycerol in the GlpF channel are also energetically costly processes. The channel achieves selectivity and conductance by provision of an amphipathic pathway that closely matches successive CH-OH groups. In GlpF, polar interactions are only possible on one side of the conducting pathway, and the hydration shell around an ion cannot be compensated for at all on the hydrophobic side. Consequently, all ions including OH-, or H_3O^+, are excluded from the channel. By also requiring a permeant group that is polarizable with both δ^+ donor, and δ^- acceptor, characteristics at each position in the selectivity filter, carbohydrates composed of CH-OH moieties are efficiently transported. Thus, the structure shows the precise mechanism for sharp selectivity and high conductance of alditols while excluding all charged species and water.

References and Notes

1. G. M. Preston *et al.*, *Science* **256**, 385 (1992).
2. C. Maurel *et al.*, *J. Biol. Chem.* **269**, 11869 (1994).
3. J. H. Park, M. H. Saier Jr., *J. Membr. Biol.* **153**, 171 (1996).
4. A. Finkelstein, *Water Movement Through Lipid Bilayers, Pores, and Plasma Membranes: Theory and Reality* (Wiley, New York, 1987).
5. K. B. Heller, E. C. Lin, T. H. Wilson, *J. Bacteriol.* **144**, 274 (1980).
6. G. M. Pao *et al.*, *Mol. Microbiol.* **5**, 33 (1991).
7. G. J. Wistow, M. M. Pisano, A. B. Chepelinsky, *Trends Biochem. Sci.* **16**, 170 (1991).
8. T. L. Anthony *et al.*, *Mol. Pharmacol.* **57**, 576 (2000).
9. A. Engel, Y. Fujiyoshi, P. Agre, *EMBO J.* **19**, 800 (2000).
10. B. L. Smith, P. Agre, *J. Biol. Chem.* **266**, 6407 (1991).
11. A. Cheng *et al.*, *Nature* **387**, 627 (1997).
12. H. Li, S. Lee, B. K. Jap, *Nature Struct. Biol.* **4**, 263 (1997).
13. L. Hasler *et al.*, *J. Mol. Biol.* **279**, 855 (1998).
14. P. Ringler *et al.*, *J. Mol. Biol.* **291**, 1181 (1999).
15. T. Walz *et al.*, *Nature* **387**, 624 (1997).
16. K. Mitsuoka *et al.*, *J. Struct. Biol.* **128**, 34 (1999).
17. J. B. Heymann, A. Engel, *J. Mol. Biol.* **295**, 1039 (2000).
18. C. Maurel, J. Reizer, J. I. Schroeder, M. J. Chrispeels, *EMBO J.* **12**, 2241 (1993).
19. D. Walther, F. Eisenhaber, P. Argos, *J. Mol. Biol.* **255**, 536 (1996).
20. G. M. Preston *et al.*, *Science* **265**, 1585 (1994).
21. M. M. Javadpour *et al.*, *Biophys. J.* **77**, 1609 (1999).
22. P. Lauger, H. J. Apell, *Biophys. Chem.* **16**, 209 (1982).
23. V. Lagree *et al.*, *J. Biol. Chem.* **273**, 12422 (1998).
24. J. D. Bernal, R. H. Fowler, *J. Chem. Phys.* **1**, 515 (1933).
25. D. Eisenberg, W. Kauzman, *The Structure and Properties of Water* (Oxford Univ. Press, London, 1969).
26. G. V. Prasad *et al.*, *J. Biol. Chem.* **273**, 33123 (1998).
27. M. J. Borgnia *et al.*, *J. Mol. Biol.* **291**, 1169 (1999).
28. P. M. Deen *et al.*, *J. Clin. Invest* **95**, 2291 (1995).
29. A. J. Yool, W. D. Stamer, J. W. Regan, *Science* **273**, 1216 (1996).
30. M. Yasui *et al.*, *Nature* **402**, 184 (1999).
31. O. S. Andersen, R. E. d. Koeppe, *Physiol. Rev.* **72**, S89 (1992).
32. L. J. Mullins, *J. Gen. Physiol.* **42**, 817 (1959).
33. D. A. Doyle, B. A. Wallace, *J. Mol. Biol.* **266**, 963 (1997).
34. D. A. Doyle *et al.*, *Science* **280**, 69 (1998).
35. G. Chang *et al.*, *Science* **282**, 2220 (1998).
36. B. Roux, R. MacKinnon, *Science* **285**, 100 (1999).
37. CCP4, *Acta Crystallogr. D* **50**, 760 (1994).
38. E. LaFortelle, J. J. Irwin, G. Bricogne, in *Crystallographic Computing 7*, P. Bourne, K. D. Watenpaugh, Eds. (Oxford Univ. Press, London, 1997).
39. A. T. Brünger, *X-PLOR Version 3.843* (Yale University, New Haven, CT, 1996).
40. N. Guex, M. C. Peitsch, *Electrophoresis* **18**, 2714 (1997).
41. http://www.povray.org
42. F. Szoka Jr., D. Papahadjopoulos, *Annu. Rev. Biophys. Bioeng.* **9**, 467 (1980).
43. P. C. Maloney, S. V. Ambudkar, *Arch. Biochem. Biophys.* **269**, 1 (1989).
44. P. Agre *et al.*, *Methods Enzymol.* **294**, 550 (1999).

45. We thank T. Earnest for help and support at the Advanced Light Source (ALS), Lawrence Berkeley National Laboratory, J. Newdoll (www.brushwithscience.com) for help with figure preparation and text, and J. Finer Moore for advice. We also thank D. Akhavan for help with Table 2 and S. Sine and P. Maloney for discussions. Supported by NIH grant GM24485 (R.M.S.). D.F. and A.L. received postdoctoral support from NIH. P.N. received postdoctoral support from the Human Frontiers Research Science Organization (grant LT0156/1999-M). Coordinates of the structure have been deposited in the Research Collaboratory for Structural Bioinformatics (RCSB) Protein Data Bank (accession code1FX8.)

11 May 2000; accepted 25 September 2000

Control of Viremia and Prevention of Clinical AIDS in Rhesus Monkeys by Cytokine-Augmented DNA Vaccination

Dan H. Barouch,[1]* Sampa Santra,[1] Jörn E. Schmitz,[1] Marcelo J. Kuroda,[1] Tong-Ming Fu,[2] Wendeline Wagner,[3] Miroslawa Bilska,[4] Abie Craiu,[1] Xin Xiao Zheng,[1] Georgia R. Krivulka,[1] Kristin Beaudry,[1] Michelle A. Lifton,[1] Christine E. Nickerson,[1] Wendy L. Trigona,[2] Kara Punt,[2] Dan C. Freed,[2] Liming Guan,[2] Sheri Dubey,[2] Danilo Casimiro,[2] Adam Simon,[2] Mary-Ellen Davies,[2] Michael Chastain,[2] Terry B. Strom,[1] Rebecca S. Gelman,[5] David C. Montefiori,[4] Mark G. Lewis,[3] Emilio A. Emini,[2] John W. Shiver,[2] Norman L. Letvin[1]

With accumulating evidence indicating the importance of cytotoxic T lymphocytes (CTLs) in containing human immunodeficiency virus–1 (HIV-1) replication in infected individuals, strategies are being pursued to elicit virus-specific CTLs with prototype HIV-1 vaccines. Here, we report the protective efficacy of vaccine-elicited immune responses against a pathogenic SHIV-89.6P challenge in rhesus monkeys. Immune responses were elicited by DNA vaccines expressing SIVmac239 Gag and HIV-1 89.6P Env, augmented by the administration of the purified fusion protein IL-2/Ig, consisting of interleukin-2 (IL-2) and the Fc portion of immunoglobulin G (IgG), or a plasmid encoding IL-2/Ig. After SHIV-89.6P infection, sham-vaccinated monkeys developed weak CTL responses, rapid loss of $CD4^+$ T cells, no virus-specific $CD4^+$ T cell responses, high setpoint viral loads, significant clinical disease progression, and death in half of the animals by day 140 after challenge. In contrast, all monkeys that received the DNA vaccines augmented with IL-2/Ig were infected, but demonstrated potent secondary CTL responses, stable $CD4^+$ T cell counts, preserved virus-specific $CD4^+$ T cell responses, low to undetectable setpoint viral loads, and no evidence of clinical disease or mortality by day 140 after challenge.

Recent studies have demonstrated the critical role of virus-specific $CD8^+$ CTL responses in controlling HIV-1 replication in humans and simian immunodeficiency virus (SIV) replication in rhesus monkeys (*1–5*). It is therefore widely believed that candidate HIV-1 vaccines should elicit potent virus-specific CTL responses. Plasmid DNA vaccination is capable of eliciting both humoral and cellular immune responses (*6–8*). DNA vaccine-elicited immune responses have protected nonhuman primates against challenges with nonpathogenic AIDS viruses (*9, 10*) and have afforded a degree of protection against pathogenic viral challenges (*11, 12*).

Boosting a DNA-primed immune response with a live recombinant vector has been shown to augment CTL responses and confer control of nonpathogenic viral challenges (*13–16*). Plasmid IL-2 has also been shown to augment DNA vaccine-elicited immune responses in a variety of murine disease